Romanian Reports in Physics **71**, 411 (2019)

DEFECT MODES SUPPORTED BY PARITY-TIME-SYMMETRIC TRIANGULAR OPTICAL LATTICES WITH SELF-DEFOCUSING KERR NONLINEARITY

HONG WANG[1,2,*], XIAOPING REN[1], DUMITRU MIHALACHE[3], YUANHANG WENG[1], JING HUANG[1], YINGJI HE[4]

[1] South China University of Technology, School of Electronics and Information Engineering, Engineering Research Center for Optoelectronics of Guangdong Province, Guangzhou, 510640, China
[2] South China University of Technology, Zhongshan Institute of Modern Industrial Technology, Zhongshan 528437, China
[3] "Horia Hulubei" National Institute for Physics and Nuclear Engineering, P.O. Box MG-6, RO-077125, Bucharest-Magurele, Romania
[4] Guangdong Polytechnic Normal University, School of Photoelectric Engineering, Guangzhou 510665, China
[*] Corresponding author: *phhwang@scut.edu.cn*

Received May 9, 2019

Abstract. The existence, stability, and evolution dynamics of fundamental and vortex solitons in parity-time-symmetric triangular optical lattices with self-defocusing Kerr (cubic) nonlinearities and single-site defects are studied. It is shown that the defect depth has a great effect on solitons' properties. For fundamental defect solitons, the existence regions shrink sharply with the decrease of the defect depth. Their stability is in accordance with the anti-Vakhitov-Kolokolov criterion. For vortex defect solitons, the positive defect plays a stabilizing role on solitons. The influence of the gain/loss component on the key characteristics of defect solitons is also presented.

Key words: defect solitons, triangular optical lattices, parity-time-symmetry.

1. INTRODUCTION

When light propagates in periodic optical lattices with a local defect, band-gap guidance can lead to the formation of both linear and nonlinear defect modes [1, 2]. Over the past decades, such defect modes have aroused intensive studies due to their potential applications in routing of optical signals [3], all-optical switching devices [4], filtering [5], and steering of optical beams [6–8]. In particular, the existence, stability, and propagation dynamics of both one- and two-dimensional defect solitons in periodic optical lattices have been investigated [9–15]. In addition, various types of photonic lattices, such as superlattices [16], square lattices [17], kagome lattices [18], and triangular lattices [19], have been reported to support robust defect solitons. However, all these studies were focused on the defect modes in conservative physical systems.

In 1998, Bender and Boettcher have shown that non-Hermitian Hamiltonians can exhibit entirely real spectra if they obey parity-time (PT)-symmetry [20]. In optics, PT-symmetric potentials can be realized by introducing a complex refractive-index distribution $n(x) = n_0 + n_R(x) + in_I(x)$ into the waveguide system, where n_0 is the background refractive index, $n_R(x)$ is the real refractive index profile of the lattice, $n_I(x)$ represents the periodic gain or loss spatial distribution of the waveguide structure [21–23], and the PT-symmetry requires that $n_R(x)$ is an even function, whereas $n_I(x)$ is an odd one. For PT-symmetric external potentials, there exists a phase transition point, above which the eigenvalues of the PT-symmetric potential are no longer purely real, but below which all eigenvalues are real [20, 23–25]. Such PT-symmetric potentials have been realized experimentally [24, 25], and the PT-symmetry breaking has been observed in experiments [25]. Interestingly, when light propagates in optical lattices with PT-symmetry, many new features such as double refraction, power oscillations etc., will be exhibited [26]. Thus, various types of solitons supported by diverse optical potentials with PT-symmetry have been extensively reported. For example, in the context of PT-symmetry, solitons in nonlinear lattices [27–29], linear lattices [22–23, 30], and mixed linear-nonlinear lattices [31, 32] have been studied in detail. The existence, stability, and propagation dynamics of fundamental [33], multi-peak [34, 35], and vortex [36] solitons in two-dimensional PT-symmetric potentials have been also investigated. Furthermore, the evolution dynamics of defect solitons in both one-dimensional [37–42] and two-dimensional [43] optical lattices with PT-symmetry has also been widely analyzed. However, all these studies of nonlinear defect modes have been concentrated on fundamental defect solitons.

For the sake of completeness, we also refer here to a few review papers in the broad research area of PT-symmetric structures and their applications [44–47] and to some recent works on PT-symmetric solitons in various relevant physical settings [48–53].

In this paper, we investigate the existence, stability, and dynamical evolution of families of fundamental and vortex solitons in PT-symmetric triangular optical lattices with single site defects, in the case of self-defocusing cubic (Kerr) optical nonlinearity. It is found that the defect depth has a great influence on the existence and stability of these nonlinear defect modes. For fundamental modes, the existence regions of defect solitons shrink with decreasing the defect depth and there exists a critical defect depth, below which no fundamental solitons can be found. It is shown that both the zero and negative defect solitons can only exist in the first gap, while positive defect solitons can exist in both semi-infinite and first gaps. For fundamental defect solitons, their stability is in accordance with the anti-Vakhitov-Kolokolov (anti-VK) criterion. For vortex cases, all defect solitons exist in the first gap, while their domains of stability expand with increasing the value of defect depth. When the defect depth is negative, all defect vortex solitons are

unstable. Thus, the positive defect depth can stabilize the vortex solitons. Moreover, the gain/loss component of PT-symmetric potential has also a great effect on the stability domains of these defect modes. It is found that tails around the soliton tend to appear and the stable regions of the soliton shrink sharply by increasing the gain/loss component. In fact, the gain/loss component plays a destabilizing role on the solitons.

The rest of the paper is organized as follows. In Section 2 we discuss the theoretical model and briefly present the method used to investigate the linear stability of nonlinear defect modes. Section 3 presents the results of numerical simulations of the existence, stability, and evolution dynamics of both fundamental and vortex defect modes, which are supported by PT-symmetric triangular lattices with self-defocusing Kerr nonlinearity. Finally, we summarize the obtained results in Sec. 4.

2. THE MODEL AND THE LINEAR STABILITY ANALYSIS

We consider a light beam propagating in two-dimensional PT-symmetric optical lattices with Kerr (cubic) nonlinearity described by the following normalized nonlinear Schrödinger equation [23]:

$$iU_z + U_{xx} + U_{yy} + 2V_0\left[V(x,y) + iW(x,y)\right] + \gamma|U|^2 U = 0, \tag{1}$$

where U is the slowly varying amplitude of the beam, z is the normalized longitudinal coordinate, (x, y) are the normalized distances along the two transverse directions, $\gamma = \pm 1$ ($\gamma = 1$ for the self-focusing nonlinearity whereas $\gamma = -1$ for the self-defocusing nonlinearity), $V(x, y)$ and $W(x, y)$ are related to the real and imaginary parts of the complex-valued refractive-index distribution, respectively, which are described as:

$$V(x,y) = \left[\frac{2}{3} + \cos\left(\vec{k}_{11}\cdot\vec{r}\right) + \cos\left(\vec{k}_{12}\cdot\vec{r}\right) + \cos\left(\vec{k}_{13}\cdot\vec{r}\right)\right]\left\{1 + \varepsilon\exp\left[-\left(x^2+y^2\right)^4\right]\right\} \tag{2}$$

$$W(x,y) = W_0\left[\sin\left(\vec{k}_{11}\cdot\vec{r}\right) + \sin\left(\vec{k}_{12}\cdot\vec{r}\right) + \sin\left(\vec{k}_{13}\cdot\vec{r}\right)\right] \tag{3}$$

with $\vec{k}_{11} = k_0\left(1, 1/\sqrt{3}\right)$, $\vec{k}_{11} = k_0\left(1, -1/\sqrt{3}\right)$, $\vec{k}_{11} = k_0\left(0, -2/\sqrt{3}\right)$, and $\vec{r} = (x, y)$.

Here V_0 controls the depth of the PT-symmetric lattices and W_0 corresponds to the amplitude of the imaginary part compared with the real part, $k_0 = 2\pi / d$, d is the period of the optical lattice, and ε represents the defect depth of the lattice. In Eq. (2), $\varepsilon > 0$, $\varepsilon = 0$, and $\varepsilon < 0$ correspond to positive, zero, and negative defects,

respectively. The intensity distributions of lattice potentials with zero, positive, and negative defects are shown in Fig. 1a, b, and c, respectively.

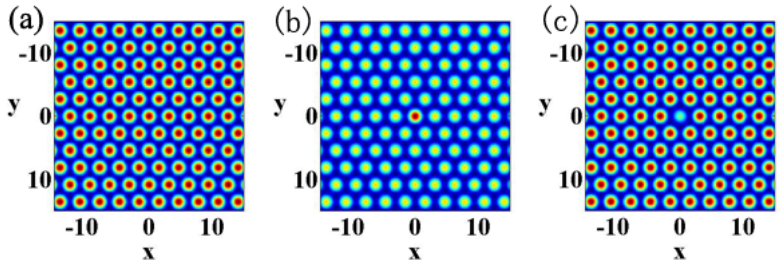

Fig. 1 – (Color online). The lattice potentials have a defect at the center with: a) $\varepsilon = 0$; b) $\varepsilon = 0.5$; c) $\varepsilon = -0.5$.

In order to get the band structure, we set $\varepsilon = 0$ and substitute

$$U(x,y,z) = u(x,y)\exp\left[i\left(k_x x + k_y y\right) + i\mu z\right] \tag{4}$$

into the linear version of Eq. (1) and obtain the following equation:

$$\left(\partial_x + ik_x\right)^2 u + \left(\partial_y + ik_y\right)^2 u + V(x,y)u = \mu u, \tag{5}$$

where $u(x, y)$ is a periodic function having the same periodicity with the lattices, μ is the propagation constant, and k_x and k_y are the wave numbers in the first Brillouin zone. We study Eq. (5) using the plane wave expansion method and get the band structure of the lattice with $\varepsilon = 0$. The corresponding band structure is displayed in Fig. 2. From Fig. 2b, we see that the band gaps shrink as long as W_0 increases and all the Bloch bands merge when $W_0 = 1$ (*i.e.*, at the phase transition point).

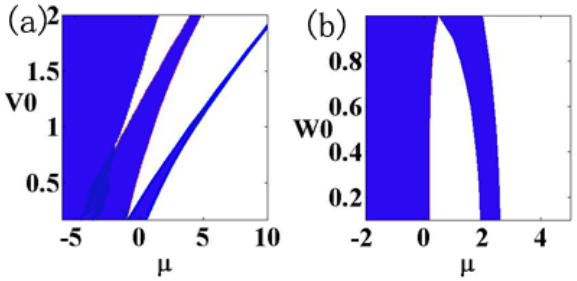

Fig. 2 – (Color online). The band structure of the PT-symmetric triangular optical lattices with $\varepsilon = 0$ (blue regions correspond to Bloch bands and the white ones represent the bandgaps): a) fixing $W_0 = 0.1$, V_0 varies from 1/6 to 2; b) fixing $V_0 = 2/3$, W_0 varies from 0.1 to 1.

The stationary soliton solutions of Eq. (1) are sought in the form of $U(x, y, z) = u(x, y) \exp(i\mu z)$, where $u(x, y)$ is a complex-valued function obeying the following nonlinear equation:

$$-\mu u + u_{xx} + u_{yy} + Vu + \gamma |u|^2 u = 0. \tag{6}$$

Equation (6) can be resolved numerically by the modified squared operator iteration method (MSOM) [54]. The total power P of the soliton is defined as $P = \int_{-\infty}^{\infty} \int_{-\infty}^{\infty} |u|^2 \mathrm{d}x\mathrm{d}y$.

In order to examine the linear stability of defect solitons, we search the perturbed solutions of Eq. (1) in the form:

$$U(x, y, z) = \left\{ u(x, y) + \left[p(x, y) - q(x, y) \right] e^{\lambda z} + \left[p(x, y) + q(x, y) \right]^* e^{\lambda^* z} \right\} e^{i\mu z}, \tag{7}$$

where $|p| << |u|, |q| << |u|$, and the superscript "*" stands for the complex conjugation. Substituting Eq. (7) into Eq. (1) and linearizing it, we obtain the following coupled equations:

$$\begin{cases} i\lambda p = -\mu q + q_{xx} + q_{yy} + 2V_0 V q - 2iV_0 W p + 2\gamma |u|^2 q - \frac{1}{2}\gamma (u^2 - (u^*)^2) p - \frac{1}{2}\gamma (u^2 + (u^*)^2) q \\ i\lambda q = -\mu p + p_{xx} + p_{yy} + 2V_0 V p - 2iV_0 W q + 2\gamma |u|^2 p + \frac{1}{2}\gamma (u^2 + (u^*)^2) p + \frac{1}{2}\gamma (u^2 - (u^*)^2) q \end{cases} \tag{8}$$

The unstable growth rate Re(λ) can be obtained numerically by the Fourier collocation method [55]. If Re(λ) > 0, the defect solitons are linearly unstable; otherwise they are linearly stable.

3. NUMERICAL RESULTS

First, we consider the fundamental defect solitons that form in PT-symmetric triangular optical lattices. For this type of solitons, we take $\varepsilon = -0.5$, $\varepsilon = -0.2$, $\varepsilon = 0$, $\varepsilon = 0.2$, and $\varepsilon = 0.5$, as typical examples. The power curves *versus* propagation constant μ are shown in Fig. 3. From this figure, we see that the positive defect solitons can exist in both the first and the semi-infinite gaps, while negative and zero defect solitons only exist in the first gap. Moreover, their existence regions shrink with the decrease of the defect depth ε, and there exists a critical defect depth ($\varepsilon = -0.8$), below which no fundamental defect solitons can be found. In addition, it is also found that the power of these defect solitons decreases monotonically by decreasing the defect depth ε. Moreover, in the first gap, by increasing the propagation constant μ, the power of both zero and negative defect solitons decreases monotonically and the solitons can be stable in their whole existence regions, while for positive defect

solitons there exist nonzero minima in their power curves. At the left-hand side of the power minimum, the soliton power is a monotonically decreasing function of the propagation constant μ and the solitons are stable in this domain, while at the right-hand side of the power minimum, the soliton power is an increasing function of the propagation constant μ and the solitons are unstable. In the semi-infinite gap, only positive defect solitons can be found, their power decreases monotonically with the increase of propagation constant and they are all stable.

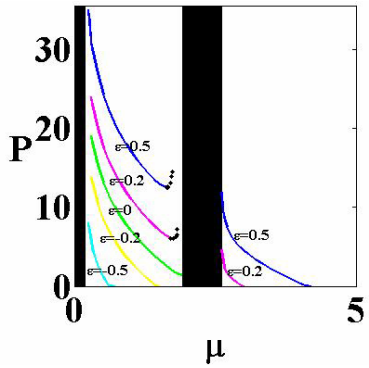

Fig. 3 – (Color online). Power diagram of fundamental defect solitons. The black shaded regions are the Bloch bands. The blue lines, magenta lines, green line, yellow line, and blue-green line correspond to stable defect solitons with $\varepsilon = 0.5$, $\varepsilon = 0.2$, $\varepsilon = 0$, $\varepsilon = -0.2$, and $\varepsilon = -0.5$, respectively. The unstable domains are plotted by black dotted lines.

To examine the longitudinal evolution of these defect modes, the robustness of solitons is numerically simulated by adding a random noise to them (10% of the soliton amplitude). For zero defect solitons we take $\mu = 1.5$ as a typical example, and their profiles at $z = 0$ and $z = 500$ are shown in Figs. 4a and 4b, respectively. From these plots, we see that the solitons can maintain their original shapes after propagating a very long distance. Furthermore, we also analyze their linear stability. It is found that the linear stability spectrum contains no unstable eigenvalues (see Fig. 4c), a result that is in accordance with the stable longitudinal evolution of these solitons, as illustrated in Figs. 4a and 4b.

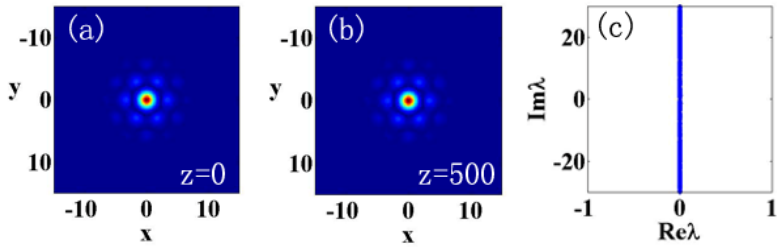

Fig. 4 – (Color online). Profiles of defect solitons at: a) $z = 0$; b) $z = 500$; c) the linear-stability spectrum of the soliton. For all cases $\mu = 1.5$ and $\varepsilon = 0$.

For positive defect solitons, fixing $\varepsilon = 0.5$, we take $\mu = 1.0$ (stable) and $\mu = 1.72$ (unstable) as typical examples in the first gap, and $\mu = 2.6$ as an example in the semi-infinite gap. The longitudinal evolution profiles and the linear-stability spectrum are shown in Figs. 5a–5c, 5d1, 5d2, 5e1, and 5e2. As the stable solitons have similar linear stability spectra as in the case of zero defect soliton shown in Fig. 4c, we only show here the linear stability spectrum of an unstable case. From Figs. 5a–5c, we see that the solitons cannot maintain their original shape at $z = 400$, and their linear-stability spectrum contains two pairs of real eigenvalues when the solitons are unstable. From Figs. 5d1, 5d2, 5e1, and 5e2, we see that the solitons can propagate robustly a long distance when they are stable.

For negative fundamental defect solitons, setting $\varepsilon = -0.5$, we take $\mu = 0.58$ as a typical example, and their evolution profiles are displayed in Figs. 5f1 and 5f2. It is obvious that these solitons propagate stably.

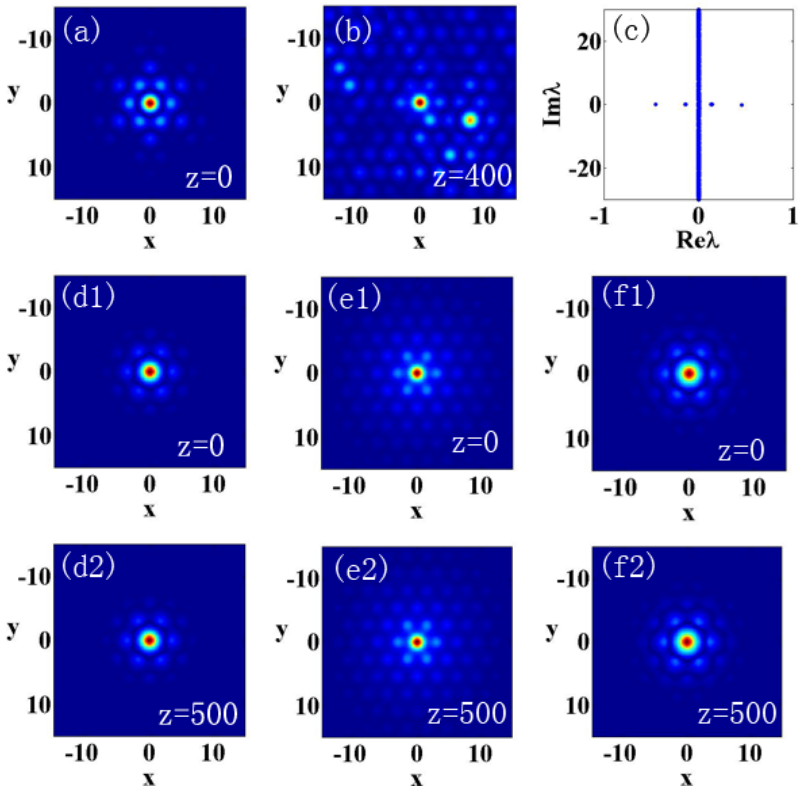

Fig. 5 – (Color online). Evolution profiles and linear-stability spectrum of positive and negative fundamental defect solitons. The upper row is for positive fundamental defect solitons with $\varepsilon = 0.5$, $\mu = 1.72$ at: a) z = 0; b) z = 400; c) is the linear-stability spectrum. For the middle and bottom rows, the first and middle column represent positive fundamental defect solitons with $\varepsilon = 0.5$, $\mu = 1.0$ and $\varepsilon = 0.5$, $\mu = 2.6$, respectively, and the last column is for negative fundamental defect solitons with $\varepsilon = -0.5$, $\mu = 0.58$.

From the above results, we see that the stability and instability domains of fundamental defect solitons in both the first and the semi-infinite gaps are in accordance with the well-known anti-Vakhitov-Kolokolov criterion [56], *i.e.*, $dP / d\mu < 0$ indicates that the solitons are stable, while $dP / d\mu > 0$ indicates that they are unstable.

Next, we will study the existence, stability, and robustness to propagation of the vortex defect solitons. Taking the parameter values $\varepsilon = 0$, $\varepsilon = 0.2$, $\varepsilon = 0.5$, and $\varepsilon = -0.2$ for zero, positive, and negative defect modes, respectively, their power diagrams are displayed in Fig. 6. Because the power curves for vortex defect solitons are quite similar, we separate them to make their observation more clear, see the four distinct panels (a)–(d) in Fig. 6. From this figure, we see that the vortex defect solitons all exist in the first gap and their domains of stability expand with the increase of defect depth.

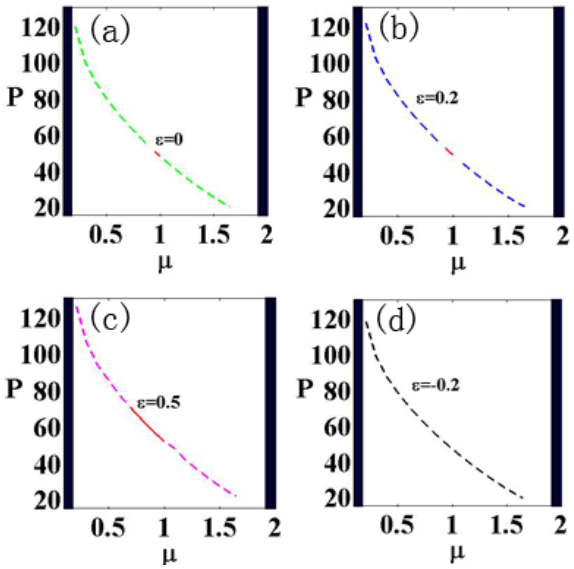

Fig. 6 – (Color online). Power curves of vortex defect solitons: a) for $\varepsilon = 0$; b) for $\varepsilon = 0.2$; c) for $\varepsilon = 0.5$; d) for $\varepsilon = -0.2$. Black shaded regions are Bloch bands. The red lines stand for stable domains, and the dashed green, blue, magenta, and black lines stand for unstable regions.

For negative vortex defect solitons, we cannot find any stable ones. This result shows that the positive defect depth can stabilize the vortex defect solitons, while the negative defect depth destabilizes them. Furthermore, it is also found that the power of all vortex defect solitons decreases with the increase of the propagation constant μ, which is very different from the case of the fundamental defect solitons.

Next, we study the inner structure of these vortex defect solitons. Taking the vortex zero defect soliton corresponding to $\mu = 1.0$ as a typical example, the real part, imaginary part, and phase are displayed in Figs. 7a–7c. The corresponding field

profile $|u|$ is shown in Fig. 7d (*i.e*. the field profile at z = 0). From these diagrams, we see that the vortex soliton has its six peaks located at six adjacent lattice sites in a regular hexagon configuration. Its center is at a lattice site that is situated between the six lattice sites. When winding around the soliton center, the phase of the soliton increases by 2π, that is the phases of the six peaks have a $\pi / 3$ difference between each other. So we can call this vortex mode the unit-charge on-site vortex soliton.

The evolution profiles and linear-stability spectra of stable and unstable cases for vortex zero defect solitons are shown in the middle row and the bottom row of Fig. 7. We see that the vortex soliton propagates stably and its linear-stability spectrum is purely imaginary when it is a stable physical object. However, the vortex soliton will become distorted during propagation and its linear-stability spectrum contains a quadruple set of complex eigenvalues when the soliton is unstable. For the vortex positive and negative defect solitons, their evolutions and linear-stability spectra are similar to those of the vortex zero defect solitons for both stable and unstable cases, so we do not discuss much hereafter.

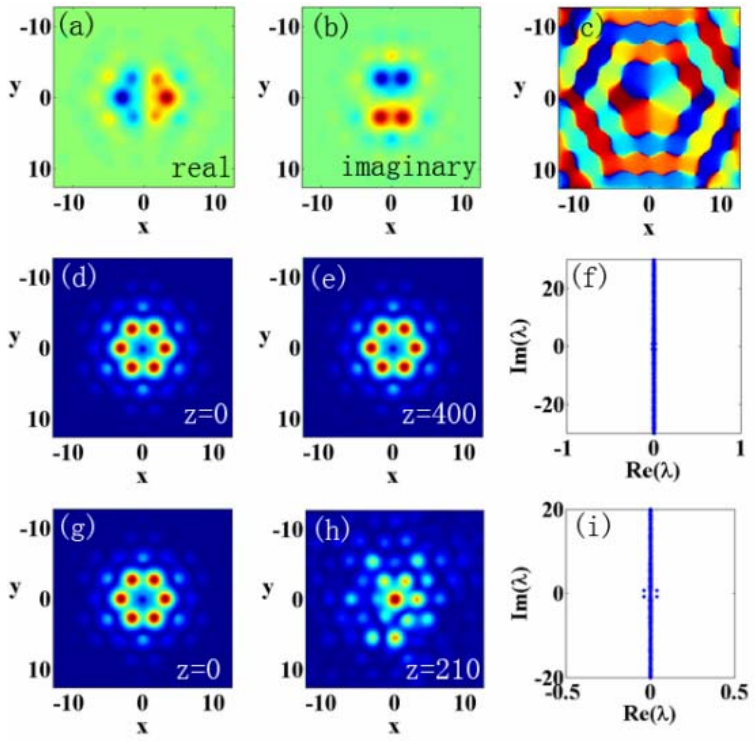

Fig. 7 – (Color online). The profile of vortex zero defect solitons and their corresponding linear-stability spectrum with: a) real part at μ 1.0; b) imaginary part at μ = 1.0; c) phase at μ = 1.0. The middle row is the evolution of vortex soliton for μ = 1.0 (stable); d) z = 0; e) z = 400; f) the corresponding linear-stability spectrum. The bottom row is for μ = 1.1 (unstable) at: g) z = 0; h) z = 210; i) the corresponding linear-stability spectrum.

Lastly, we investigate the influence of gain/loss component on the formation and stability of solitons. We take, as a typical example, the fundamental positive defect soliton with defect depth $\varepsilon = 0.5$. The corresponding field profiles $|u|$, real and imaginary parts for $V_0 = 2/3$, $W_0 = 0.1$, $\mu = 1.0$ and $V_0 = 2/3$, $W_0 = 0.8$, $\mu = 0.9$ are shown in Fig. 8. It is found that by increasing the gain/loss component, the imaginary part of the soliton becomes stronger, while the real part becomes weaker, and tails around both real and imaginary parts tend to appear, *i.e.*, the soliton becomes less localized. It is worth noting that when the gain/loss component is absent, *i.e.*, $W_0 = 0$, the imaginary part of the soliton field profile is equal to zero.

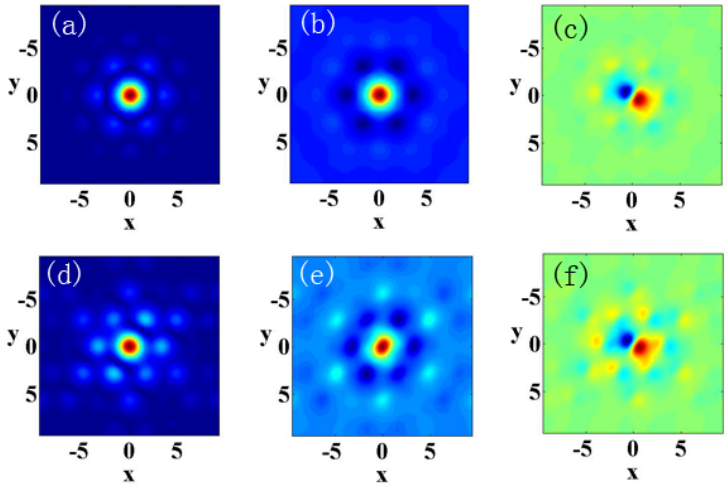

Fig. 8 – (Color online). The field profile of fundamental defect soliton with defect depth $\varepsilon = 0.5$, and $V_0 = 2/3$, the upper row is for $W_0 = 0.1$, $\mu = 1.0$ with: a) $|u|$; b) real part; c) imaginary part. The bottom row is for $W_0 = 0.8$, $\mu = 0.9$ with: d) $|u|$; e) real part; f) imaginary part.

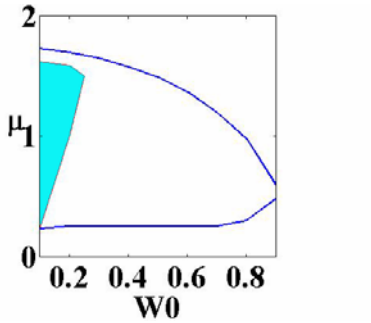

Fig. 9 – (Color online). Existence and stability domains of fundamental defect solitons in the first gap with defect depth $\varepsilon = 0.5$ *versus* gain/loss component. The region between the two blue lines is the existence domain. The shaded region is the stability domain.

We see that with the increase of gain/loss component, the soliton becomes less stable and its existence domain shrinks sharply as the strength of the imaginary

part contribution, relative to the real part contribution in the potential, is increased. We next take the fundamental defect soliton in the first gap with the defect depth $\varepsilon = 0.5$ as an example. Its domains of existence and stability *versus* the gain/loss component are displayed in Fig. 9, which indicates that the region of stability of solitons disappears quickly with the increase of the gain/loss parameter W_0.

4. CONCLUSIONS

In this paper, the evolution dynamics of both fundamental and vortex solitons in PT-symmetric triangular optical lattices with self-defocusing Kerr nonlinearity and single site defect has been studied numerically. It has been shown that the defect depth has a great influence on soliton dynamics. For fundamental defect solitons, the existence domains shrink sharply with the decrease of the defect depth. The stability of fundamental defect solitons is in perfect accordance with the anti-Vakhitov-Kolokolov criterion. For vortex defect solitons, their domains of stability expand with the increase of defect depth, which indicates that the positive defect plays a stabilizing role.

The influence of the gain/loss component on the key features of defect solitons in PT-symmetric triangular optical lattices is also investigated. It is found that the soliton field distribution is described by a real-valued function if the gain/loss component is absent, *i.e.* when the parameter $W_0 = 0$. Moreover, by increasing the gain/loss component of the external potential, tails around both real and imaginary parts of the soliton appear, and the regions of stability become narrower as the strength of the imaginary part contribution relative to the real part contribution is increased.

Acknowledgements. This work was supported by Science & Technologies Plan Projects of Guangdong Province (Nos. 2017B010112003, 2017A050506013), and Applied technologies R & D Major Projects of Guangdong Province (Nos. 2015B010127013, 2016B01012300), and Science & Technologies Plan Projects of Guangzhou City (Nos. 201604046021, 201704030139, 201905010001), Science & Technologies Development Special Fund Projects of Zhongshan City (Nos. 2017F2FC0002, 2017A1009), the Guangdong Province Nature Foundation of China (Grant No. 2017A030311025), and the Guangdong Province Education Department Foundation of China (Grant No. 2014KZDXM059).

REFERENCES

1. A. A. Sukhorukov and Y. S. Kivshar, Phys. Rev. Lett. **87**, 083901 (2011).
2. I. Makasyuk, Z. Chen, and J. Yang, Phys. Rev. Lett. **96**, 223903 (2006).
3. Y. V. Kartashov, V. A. Vysloukh, and L. Torner, Prog. Opt. **52**, 63 (2009).
4. F. Ye, Y. V. Kartashov, V. A. Vysloukh, and L. Torner, Phys. Rev. A **78**, 013847 (2008).
5. A. A. Sukhorukov and Y. S. Kivshar, Opt. Lett. **30**, 1849 (2005).
6. C. R. Rosberg, I. L. Garanovich, A. A. Sukhorukov, D. N. Neshev, W. Krolikowski, and Y. S. Kivshar, Opt. Lett. **31**, 1498 (2006).
7. A. Picardi, G. Assanto, L. Lucchetti, and F. Simoni, Appl. Phys. Lett. **93**, 171104 (2008).
8. Y. V. Kartashov, L. Torner, and V. A. Vysloukh, Opt. Lett. **29**, 1102 (2004).
9. F. Fedele, J. Yang, and Z. Chen, Stud. Appl. Math. **115**, 279 (2005).
10. J. Yang and Z. Chen, Phys. Rev. E **73**, 026609 (2006).

11. W. H. Chen, Y. J. He, and H. Z. Wang, Opt. Express **14**, 11271 (2006).
12. X. Wang, J. Young, Z. Chen, D. Weinstein, and J. Yang, Opt. Express **14**, 7362 (2006).
13. Y. Liu, Y. Guan, H. Li, Z. Luo, and Z. Mai, Opt. Commun. **397**, 105 (2017).
14. J. Wang, J. Yang, and Z. Chen, Phys. Rev. A **76**, 013828 (2007).
15. W. H. Chen, X. Zhu, T. W. Wu, and R. H. Li, Opt. Express **18**, 10956 (2010).
16. W. H. Chen, Y. J. He, and H. Z. Wang, Opt. Express **15**, 14498 (2007).
17. H. Wang, W. He, X. Zhu, and Y. J. He, Rom. Rep. Phys. **64**, 1391 (2012).
18. X. Zhu, H. Wang, and L. X. Zheng, Opt. Express **18**, 20786 (2010).
19. X. Zhu, H. Wang, T. W. Wu, and L. X. Zheng, J. Opt. Soc. Am. B **28**, 521 (2011).
20. C. M. Bender and S. Boettcher, Phys. Rev. Lett. **80**, 5243 (1998).
21. R. El-Ganainy, K. G. Makris, D. N. Christodoulides, and Z. H. Musslimani, Opt. Lett. **32**, 2632 (2007).
22. K. G. Makris, R. El-Ganainy, and D. N. Christodoulides, Phys. Rev. Lett. **100**, 103904 (2008).
23. Z. H. Musslimani, K. G. Makris, R. El-Ganainy, and D. N. Christodoulides, Phys. Rev. Lett. **100**, 030402 (2008).
24. C. E. Ruter, K. G. Makris, R. El-Ganainy, D. N. Christodoulides, M. Segev, and D. Kip, Nature Phys. **6**, 192 (2010).
25. A. Guo, G. J. Salamo, D. Duchesne, R. Morandotti, M. Volatier-Ravat, V. Aimez, G. A. Siviloglou, and D. N. Christodoulides, Phys. Rev. Lett. **103**, 093902 (2009).
26. K. G. Makris, R. El-Ganainy, D. N. Christodoulides, and Z. H. Musslimani, Phys. Rev. A **81**, 063807 (2010).
27. F. K. Abdullaev, Y. V. Kartashov, V. V. Konotop, and D. A. Zezyulin, Phys. Rev. A **83**, 041805 (2011).
28. D. A. Zezyulin, Y. V. Kartashov, and V. V. Konotop, Europhys. Lett. **96**, 64003 (2011).
29. Y. He, X. Zhu, D. Mihalache, J. Liu, and Z. Chen, Opt. Commun. **285**, 3320 (2012).
30. Z. H. Musslimani, K. G. Makris, R. El-Ganainy, and D. N. Christodoulides, J. Phys. A **41**, 244019 (2008).
31. Y. He, X. Zhu, D. Mihalache, J. Liu, and Z. Chen, Phys. Rev. A **85**, 013831 (2012).
32. Y. He and D. Mihalache, Rom. Rep. Phys. **64**, 1243 (2012).
33. J. Zeng and Y. Lan, Phys. Rev. E **85**, 047601 (2012).
34. H. Wang, S. Shi, X. Ren, X. Zhu, B. A. Malomed, D. Mihalache, and Y. He, Opt. Commun. **335**, 146 (2015).
35. X. Zhu, H. Wang, H. Li, W. He, and Y. J. He, Opt. Lett. **38**, 2723 (2013).
36. X. Ren, H. Wang, H. Wang, and Y. He, Opt. Express **22**, 19755 (2014).
37. H. Wang and J. Wang, Opt. Express **19**, 4030 (2011).
38. Z. Lu and Z. M. Zhang, Opt. Express **19**, 11457 (2011).
39. H. Wang, W. He, L. X. Zheng, X. Zhu, H. G. Li, and Y. J. He, J. Phys. B **45**, 245401 (2012).
40. S. M. Hu and W. Hu, Eur. Phys. J. D **66**, 266 (2012).
41. S. M. Hu and W. Hu, Physica B **429**, 28 (2012).
42. H. Wang, W. He, S. Shi, X. Zhu, and Y. J. He, Phys. Scr. **89**, 025502 (2014).
43. J. Xie, Z. Su, W. Chen, G. Chen, J. Lv, D. Mihalache, and Y. He, Opt. Commun. **313**, 139 (2014).
44. V. V. Konotop, J. Yang, and D. A. Zezyulin, Rev. Mod. Phys. **88**, 035002 (2016).
45. S. V. Suchkov, A. A. Sukhorukov, J. H. Huang, S. V. Dmitriev, C. Lee, and Y. S. Kivshar, Laser Photonics Rev. **10**, 177 (2016).
46. D. Mihalache, Rom. Rep. Phys. **69**, 403 (2017).
47. B. A. Malomed and D. Mihalache, Rom. J. Phys. **64**, 106 (2019).
48. B. Liu, L. Li, and B. A. Malomed, Eur. Phys. J. D **71**, 140 (2017).
49. R. J. Lombard and R. Mezhoud, Rom. J. Phys. **62**, 112 (2017).
50. R. J. Lombard, R. Mezhoud, and R. Yekken, Rom. J. Phys. **63**, 101 (2018).
51. P. Li, L. Li, and D. Mihalache, Rom. Rep. Phys. **70**, 408 (2018).
52. B. Liu, L. Li, and D. Mihalache, Rom. Rep. Phys. **70**, 409 (2018).
53. H. Wang, J. Huang, X. Ren, Y. Weng, D. Mihalache, and Y. He, Rom. J. Phys. **63**, 205 (2018).
54. J. Yang and T. I. Lakoba, Stud. Appl. Math. **118**, 153 (2007).
55. J. Yang, *Nonlinear Waves in Integrable System*, SIAM, New York, 2010.
56. H. Sakaguchi and B. A. Malomed, Phys. Rev. A **81**, 013624 (2010).